1050–1066 *Nucleic Acids Research, 2023, Vol. 51, No. 3* *Published online 20 January 2023*
https://doi.org/10.1093/nar/gkad002

A bio-orthogonal linear ubiquitin probe identifies STAT3 as a direct substrate of OTULIN in glioblastoma

Xianli Du[1,†], Jing Pang[1,†], Bin Gu[3,†], Tian Si[1], Yan Chang[4], Tianqi Li[3,5], Min Wu[2], Zicheng Wang[1], Yuxia Wang[1], Jiannan Feng[1], Ning Wu[1], Jianghong Man[2], Huiyan Li[2], Ailing Li[2], Tong Zhang[3,*], Bo Wang[1,*] and Xiaotao Duan[1,2,*]

[1]State Key Laboratory of Toxicology and Medical Countermeasures, Beijing Institute of Pharmacology and Toxicology, Beijing 100850, China, [2]State Key Laboratory of Proteomics, National Center of Biomedical Analysis, Beijing 100850, China, [3]Department of Stomatology, the First Medical Center, Chinese PLA General Hospital, Beijing 100853, China, [4]Beijing Key Laboratory for Pediatric Diseases of Otolaryngology, Head and Neck Surgery, MOE Key Laboratory of Major Diseases in Children, Beijing Pediatric Research Institute, Beijing Children's Hospital, Capital Medical University, National Center for Children's Health, Beijing 100045, China and [5]Medical School of Chinese PLA, Beijing 100853, China

Received April 13, 2022; Revised November 23, 2022; Editorial Decision December 22, 2022; Accepted January 03, 2023

ABSTRACT

While linear ubiquitin plays critical roles in multiple cell signaling pathways, few substrates have been identified. Global profiling of linear ubiquitin substrates represents a significant challenge because of the low endogenous level of linear ubiquitination and the background interference arising from highly abundant ubiquitin linkages (e.g. K48- and K63-) and from the non-specific attachment of interfering proteins to the linear polyubiquitin chain. We developed a bio-orthogonal linear ubiquitin probe by site-specific encoding of a norbornene amino acid on ubiquitin (NAEK-Ub). This probe facilitates covalent labeling of linear ubiquitin substrates in live cells and enables selective enrichment and identification of linear ubiquitin-modified proteins. Given the fact that the frequent overexpression of the linear linkage-specific deubiquitinase OTULIN correlates with poor prognosis in glioblastoma, we demonstrated the feasibility of the NAEK-Ub strategy by identifying and validating substrates of linear ubiquitination in patient-derived glioblastoma stem-like cells (GSCs). We identified STAT3 as a bona fide substrate of linear ubiquitin, and showed that linear ubiquitination negatively regulates STAT3 activity by recruitment of the phosphatase TC-PTP to STAT3. Furthermore, we demonstrated that preferential expression of OTULIN in GSCs restricts linear ubiquitination on STAT3 and drives persistent STAT3 signaling, and thereby maintains the stemness and self-renewal of GSCs.

GRAPHICAL ABSTRACT

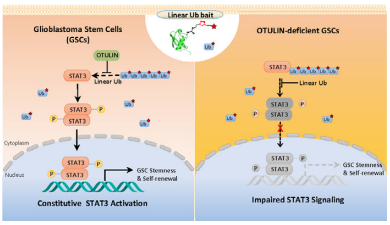

INTRODUCTION

Protein linear ubiquitination is an atypical post-translational modification in which the polyubiquitin (polyUb) chains are connected to lysine residues through the N-terminal methionine in a head-to-tail assembly. The homeostasis of linear ubiquitination is tightly regulated by the linear Ub assembly complex (LUBAC, composed of HOIP, HOIL-1L and SHARPIN) (1–4) and the specific deubiquitinase OTULIN (also known as FAM105B or Gumby) (5–7). Aberrant linear ubiquitination accounts for a range of immune dysfunctions and inflammatory diseases (8).

A handful of immune- and inflammation-related proteins have been identified as linear Ub-modified substrates, such as the core element of the NF-κB complex NEMO

*To whom correspondence should be addressed. Email: xduan@ncba.ac.cn
Correspondence may also be addressed to Bo Wang. Email: wangbo1@bmi.ac.cn
Correspondence may also be addressed to Tong Zhang. Email: kqzhengji301@163.com
†The authors wish it to be known that, in their opinion, the first three authors should be regarded as Joint First Authors.

(2,9), the inflammasome adaptor protein ASC (10), the necroptosis mediator RIPK1 (11) and the essential component of interferon signaling STAT1 (12). These previously identified substrates are well established to have linear Ub as an essential regulator of innate and adaptive immunity. Our group recently reported that the linear Ub chain directly modifies the mitotic motor CENP-E and controls chromosome alignment (13). This finding links aberrant linear ubiquitination to cell cycle arrest and tumorigenesis. Systematic exploration of linear ubiquitination is just at its beginning, as many more substrates of linear Ub are yet to be identified. Therefore, a global analysis of linear Ub-modified proteins, preferably in a live cell context, will not only expand our knowledge concerning the functional diversity of linear ubiquitination but will also provide new insights into mechanisms of linear Ub signaling.

As the abundance of linear ubiquitinated species is generally too low to be directly detected [e.g. by mass spectrometry (MS)], strategies that can specifically enrich the linear Ub-modified substrates are required. Conventional pull-down assays, using either commercial antibodies (14,15) or linear Ub-binding domains (9), showed insufficient affinity and specificity towards linear Ub substrates. They usually suffered from non-specific binding of interfering proteins to polyUb chains and/or from cross-reactivity towards the high background Ub linkages (i.e. K48- and K63-linked polyubiquitination). Koraljka Husnjak and coworkers introduced an internal tag onto Ub, allowing enrichment of linear Ub substrates from cellular matrices (16). Nonetheless, the fusion tag (STREP II, an 11 amino acid peptide) is relatively large compared with natural Ub. Furthermore, the peptide tag introduced a new lysine residue, which adds another layer of complexity of Ub assembly.

We present here a live cell-compatible bio-orthogonal strategy to capture the direct linear polyUb-modified substrates. We constructed a linear Ub-specific probe by internally incorporating a non-canonical amino acid [Nε-2-azidoethyloxycarbonyl-L-lysine (NAEK)] into Ub via genetic code expansion. This engineered Ub probe shows minimal structural difference compared with native Ub and, thereby, preserves the conjugation of linear Ub chains well. When combined with click chemistry and MS, this probe enables capture and identification of substrates of linear Ub with improved specificity and accuracy. As a proof-of-concept, we applied this bio-orthogonal strategy to the profiling of linear Ub substrates in patient-derived glioblastoma stem-like cells (GSCs), an aggressive population of glioblastoma cells that display a high capacity for self-renewal and therapeutic resistance. We identified STAT3 as a bona fide substrate of linear Ub, and showed that linear ubiquitination impairs STAT3 activity by recruitment of its phosphatase TC-PTP (T-cell protein tyrosine phosphatase) in GSCs. Moreover, we demonstrated that the linear linkage-specific deubiquitinase OTULIN maintains the stemness and self-renewal of GSCs via restricting STAT3 linear ubiquitination, and thereby serves as a promising therapeutic target for glioblastoma.

MATERIALS AND METHODS

Common reagents and antibodies

The following reagents were purchased from commercial sources: human interleukin-6 (IL-6; SRP3096, Sigma), phosSTOP phosphatase inhibitor (4906837001, Roche), protease inhibitor cocktail (493132001, Roche), TurboFect Transfection Reagent (R0532, Thermo Fisher), normal rabbit IgG (12-370, Merck-millipore), normal mouse IgG (61656, CST), UBE1 (E-305-025, Boston Biochem), UBE2D3 (E2-627, Boston Biochem), UBE2L3 (E2-640, Boston Biochem), recombinant human OTULIN protein (E-558, Boston Biochem), recombinant human Ub (U-100H, Boston Biochem), RNF31 catalytic domain (E3-240-100, R&D), recombinant GST–STAT3 (ab43618, Abcam), ubiquitin conjugation reaction buffer (Sk-10, Boston Biochem), L-glutathione reduced (G8180, Solarbio), RNAiMAX Transfection Reagent (13778150, Invitrogen), biotin sDIBO Alkyne (C20023, Invitrogen), Pierce™ High Capacity Streptavidin Agarose (20359, Thermo Fisher), enterokinase (NEB, P8070s), enzyme-linked chemiluminescence (ECL) plus (32132, Thermo Fisher), Opti-MEM™ (31985070, Gibco), Sosoo cloning kit (TSV-s2, Tsingke), protein A–Sepharose (17-1279-01, GE), NAEK (A848920, J&K), Flag M2 beads (A2220, Sigma), Pierce™ BCA Protein Assay Kit (23225, Thermo Fisher), 4–12% SurePAGE Bis-Tris gel (GenScript, M00654), NE-PER™ Nuclear and Cytoplasmic Extraction Reagents (78835, Thermo Fisher), Dual-Glo® Luciferase Assay System (E2940, Promega), CellTiter-Glo® Luminescent Cell Viability Assay (E7572, Promega), FITC Annexin V (640905, biolegend) and recombinant human IL-1β (200-01B, Peprotech).

Antibodies were as follows: mouse anti-Myc (1:1000, Sc-40, Santa Cruz), mouse anti-HA (sc-7392, Santa Cruz), mouse anti-Flag (F3156, Sigma), Dylight 488 (GR3248444-2, Abcam), rabbit anti-HOIP (99633S, CST), sheep anti-HOIL-1 (a gift from Dr Philip Cohen), rabbit anti-SHARPIN (12541S, CST), rabbit anti-STAT3 (4904S, CST), mouse anti-STAT3 (9139S, CST), rabbit anti-Phospho-STAT3 (Y705) (9145S, CST), rabbit anti-Ub (ab33893, Abcam), rabbit anti-Ub-K48 (12805S, CST), rabbit anti-Ub-K63 (12930S, CST), human anti-linear Ub (14) (a gift from Dr Vishva M. Dixit, Genentech Inc.), rabbit anti-UBE2D3 (4330S, CST), rabbit anti-OTULIN (ab15117, Abcam), mouse anti-α-tubulin (T5168, Sigma), mouse anti-OLIG2 (66513, Proteintech), mouse anti-SOX2 (Sc-365823, Santa Cruz), rabbit anti-GFAP (12389S, CST), rabbit anti-Lamin B1 (A16909, Abclonal), rabbit anti-caspase 3 (14220, CST) and rabbit anti-PARP (9542, CST).

Biological resources

Human HEK293T cells purchased from the ATCC, and stat3-null HeLa cells purchased from ABclonal (20170728-02) were grown in Dulbecco's modified Eagle's medium (DMEM) with 10% fetal bovine serum (FBS; FND500, excellbio), 100 U/ml penicillin and 100 U/ml streptomycin. GSC lines were obtained from Professor Jeremy N. Rich (University of California San Diego). GSCs were cultured

in Neurobasal™ medium (12348017, Gibco) supplied with B27 supplement (12587010, Gibco), 10 ng/ml epidermal growth factor (EGF) and 10 ng/ml fibroblast growth factor (FGF) as previously described (17,18). All cell lines were used for a limited number of passages and checked for Mycoplasma infection.

PylRS/tRNA translation system

The expression cassette of four-copy 7SK-tRNA was amplified from the 7SK-tRNA-PylRS vector (19) and inserted into the pCDH-EF1-MCS lentiviral vector at the SpeI restriction sites, to generate pCDH-7SK-tRNA-EF1-MCS. The MbPylRS gene was amplified from the 7SK-tRNA-PylRS vector and inserted downstream of the EF1 promotor between the XbaI and BamHI restriction sites in pCDH-7SK-tRNA-EF1-MCS, to generate pCDH-7SK-tRNA-EF1-PylRS. pCDH-U6-tRNA-EF1-Ub-54TAG was constructed with a similar strategy. The Ub-54TAG gene was amplified and inserted downstream of the EF1 promoter between the XbaI and BamHI restriction sites in the pCDH-EF1-MCS lentiviral vector, to generate pCDH-EF1-NAEK-Ub. In order to obtain a high transcription level of tRNA, a U6-tRNA cassette in which tRNA was driven by the U6 promoter was synthesized and inserted upstream of the EF1 promoter in an opposite orientation at the SpeI restriction site in pCDH-EF1-NAEK-Ub.

Preparation of recombinant NAEK-Ub

Recombinant NAEK-Ub was purified from HEK293T cells. We constructed a NAEK-Ub expression vector encoding glutathione *S*-transferase (GST)–Ub-54TAG, in which an enterokinase cleavage site was induced at the 5′ terminus of the Ub-54TAG gene. The 7SK-tRNA-PylRS vector and NAEK-Ub expression vector were co-transfected into HEK293T cells by TurboFect transfection reagent. NAEK (1 mM, A848920, J&K) was added to the culture medium to provide the unnatural amino acid. In total 5×10^9 HEK293T cells were collected and lysed in RIPA buffer containing 20 mM Tris–HCI pH 7.5, 150 mM NaCl, 10 mM EDTA, 1% Triton X-100, 1% deoxycholate, 1 mM phenylmethylsulfonyl fluoride (PMSF), complete protease inhibitor and 20 mM *N*-ethylmaleimide (E3876, Sigma). Cell lysates were sonicated and centrifuged at 12 000 rpm. The supernatants were co-incubated with GST-beads (20507ES10, Yeasen ShangHai) and the recombinant GST–NAEK-Ub was pulled down following the manufacturer's protocol. The eluted protein was then digested by enterokinase (NEB, P8070s) and further purified by size-exclusion chromatography (GE). The protein was concentrated by ultrafiltration using Amicon Ultra-4 (Merck Milipore, 1500G, 30 min). Protein concentrations in this study were measured and adjusted using the Pierce™ BCA Protein Assay Kit (23225, Thermo Fisher).

In vitro ubiquitin chain assembly assay

The enzymes UBE1, UBE2D3 and $HOIP^{RBR\text{-}LDD}$ were purchased from Boston Biochem. The recombinant NAEK-Ub was purified as described above. The Ub conjugation reactions were prepared by mixing 100 nM UBE1, 600 nM UBE2D3, 1 μM $HOIP^{RBR\text{-}LDD}$, 15 μM GST–Ub, 15 μM Ub or NAEK-Ub in ubiquitin conjugation reaction buffer (Boston Biochem, SK-10). Reactions were performed at 37°C for 3 h with or without 2 mM ATP and stopped by the addition of protein loading buffer containing β-mercaptoethanol. Samples were separated on 4–12% sodium dodecylsulfate (SDS)–polyacrylamide gel electrophoresis (PAGE) gels (GenScript) in MES buffer and analyzed by western blot using Ub antibody and linear Ub antibody.

E2 conjugation test

The Ub conjugation to E2 enzymes was carried out as described previously (20). In detail, 1 μM wild-type Ub or NAEK-Ub was incubated with 0.2 μM UBE1 and 1 μM E2 (UBE2D3 or UBE2L3) in reaction buffer containing 20 mM Tris–HCl, pH 7.5, 50 mM NaCl and 2 mM $MgCl_2$ with or without 20 mM dithiothreitol (DTT) at 37°C for 15 min. The reactions were initiated by the addition of 2 mM ATP and stopped by the addition of non-reducing/reducing SDS–PAGE loading buffer. The reaction mixtures were boiled for 10 min before being subjected to 4–12% SDS–PAGE (GenScript) in MES buffer and analyzed by silver stain (Protein Silver Stain Kit, CWbio) or western blot using anti-Ub antibody and anti-UBE2D3 antibody.

Live cell labeling and NAEK-Ub pull down

GSCs were sequentially infected with lentivirus-packed pCDH-7SK-tRNA-EF1-PylRS vector and lentivirus-packed pCDH-U6-tRNA-EF1-Ub-54TAG vector. The PylRS-$tRNA_{CUA}$/Ub-54TAG engineered GSCs were infected with lentivirus carrying shOTULIN or non-targeting short hairpin RNA (shRNA) control. Puromycin (2 μg/ml) was added 72 h post-infection for antibiotic selection. The resultant GSCs were treated with NAEK (1 mM), and then harvested by centrifugation, washed twice in pre-chilled phosphate-buffered saline (PBS) and lysed in RIPA buffer (containing 20 mM Tris–HCI pH 7.5, 150 mM NaCl, 10 mM EDTA, 1% Triton X-100, 1% deoxycholate, 1 mM PMSF, complete protease inhibitor and 20 mM *N*-ethylmaleimide). The lysates were centrifuged at 13 000 rpm at 4°C for 10 min. The SPAAC reaction (i.e. strain-promoted alkyne–azide cycloaddition) was carried out by incubating the supernatants with 10 μM biotin–DIBO (dibenzylcyclooctyne; C20023, Invitrogen) at room temperature for 2 h. Streptavidin–agarose was added into the labeled supernatants and incubated overnight at 4°C, followed by washing five times. Finally, the streptavidin–agarose was boiled in 1× SDS buffer supplemented with β-mercaptoethanol for 10 min. Protein samples were separated by SDS–PAGE and then subjected to western blotting and/or MS analysis.

Serum-induced differentiation of GSCs

GSCs were cultured in stem cell medium (Neurobasal-A medium with B27 supplement, 10 ng/ml EGF and 10 ng/ml FGF) overnight, then sorted by magnetic cell sorting using the surface marker CD133 (Miltenyi Biotec,

CD133high cells), cultured in stem cell medium as described above and validated by stem cell marker expression [SRY-box 2 (SOX2) and oligodendrocyte transcription factor 2 (OLIG2)]. Differentiation of GSCs was induced by exposure to DMEM with 10% FBS, and cells were maintained in serum culture conditions (17) and assayed for the gain of differentiation marker [glial fibrillary acidic protein (GFAP)] and loss of stem cell markers (SOX2 and OLIG2).

Sphere formation assay and *in vitro* limiting dilution assay

The sphere formation assay and *in vitro* limiting dilution assay were performed as described (21). For the sphere formation assay, GSCs were plated in 96-well plates at a density of 1000 cells/well and cultured in the Neurobasal medium. Tumor sphere sizes and sphere volume were assessed on the 11th day after implantation. For *in vitro* limiting dilution assays, GSCs were seeded in 96-well plates at 2, 5, 10, 20, 40, 80 and 160 cells/well, with six replicates for each cell number. The presence of tumor spheres in each well was determined after 10 days of maintenance. Limiting dilution analysis was performed using ELDA online software (http://bioinf.wehi.edu.au/software/elda/). Each well was also evaluated for the total number of tumor spheres.

Immunofluorescence staining

GSCs were infected with lentivirus carrying Flag-STAT3 or Flag-STAT3-4KR mutations and then infected or not with lentivirus carrying pLKO.1-shOTULIN. GSCs were plated on cover glasses coated with Matrigel (Corning, 354277) in a 24-well plate at a density of 1×10^5 cells/well and incubated overnight. Cells were fixed in 4% paraformaldehyde for 20 min, and then blocked in 10% FBS with 0.3% Triton X-100 in PBS for 20 min at room temperature, followed by incubation with primary antibody Phospho-Stat3(Tyr705) (1:100, 9145S, CST) overnight at 4°C. Then cells were incubated with the secondary antibody labeled with DyLight 488 (1:100, ab96899, Abcam) for 1 h at room temperature. Nuclei were counterstained with 4′,6-diamidino-2-phenylindole (DAPI). Images were acquired on a Zeiss LSM880 system; the acquisition software was Zen 2.1 SP2.

RNA isolation and real-time PCR

Total RNA was isolated from cultured cells using the RNeasy Kit (QIAGEN). cDNA was synthesized by reverse transcription using oligo(dT) and subjected to real-time polymerase chain reaction (PCR) with human c-Myc, SOCS3 and GADPH primers in the presence of Cyber green PCR-Mix (Applied Biosystems). Data were analyzed from three independent experiments and are shown as the mean ± standard deviation (SD). Primer pairs used to detect the mRNA levels of the genes by quantitative reverse transcription–PCR (RT–qPCR) are given in Supplementary Table S7.

Circular dichroism measurement

Circular dichroism (CD) spectra were recorded on a Jasco J-815 spectropolarimeter equipped with a CDF-426S Peltier-type thermostatic cell holder. Far-UV CD spectra acquisition was performed at a protein concentration of 25 μM in 50 mM sodium phosphate buffer (pH 7.4) at 20°C using fused silica cuvettes with 1 mm path lengths (Hellma, Jena, Germany). The CD data are shown as the mean residue ellipticity, and the [θ]222-value of $-33\ 000^\circ cm^2/dmol$ was taken to correspond to 100% α-helicity.

Structural modeling

Based on the crystal structure of Ub (PDB code: 1ubq), the 3D theoretical structure was optimized using Discover_3 software (InsightII 2005 program, MSI, San Diego, CA, USA) under an extensible and systematic force field (ESFF). The chosen minimization methods was the steepest descent (20 000 steps; the convergence criterion was 0.01 kJ/mol), followed by conjugate gradient (30 000 steps; the convergence criterion was 0.01 kJ/mol). With the optimized theoretical structure of Ub as a model, the theoretical solvent-accessible surface and polarity distribution were analyzed using the Homology module of the InsightII 2005 program. With the substitution of selected amino acid residues, the 3D theoretical structures of the substitutions were modeled and optimized as the parent model. Then, the stable energy of the mutants was calculated. All modeling and calculations were performed using Insight II 2005 on an IBM workstation.

Mass spectrometric analysis

NAEK-Ub proteome identification and quantification was performed as previously described (22). MS was carried out on an Orbitrap Fusion mass spectrometer (Thermo Fisher), which was operated in the positive-ion mode at an ion transfer tube temperature of 320°C. The positive-ion spray voltage was 2.0 kV. The Orbitrap Fusion Lumos was set to the OT–IT mode. For a full MS survey scan, the target value was 5×10^5 and the scan ranged from 300 to 1400 m/z at a resolution of 120 000 and a maximum injection time of 50 ms. For the MS2 scan, a duty cycle of 3 s was set with the top-speed mode. Only spectra with a charge state of 2–6 were selected for fragmentation by higher energy collision dissociation with a normalized collision energy of 35%. The MS2 spectra were acquired in the ion trap in rapid mode with an AGC target of 7000 and a maximum injection time of 35 ms, and the dynamic exclusion was set to 18 s. The MS/MS spectra were searched against the Human UniProt FASTA database (UP000005640, containing 77027 entries) and trypsin was selected as the digestive enzyme with two potential missed cleavages. The false discovery rate (FDR) for peptides and proteins was controlled at <1% by the Andromeda search engine. The MS quantitative data were analyzed via the software MaxQuant (http://maxquant.org/, version 1.6.5.0).

Statistical analysis

Statistical comparisons were carried out by two-sided Student's *t*-test or by one-way analysis of variance (ANOVA) with Tukey's multiple comparison. Statistical calculations were performed with SPSS software. For all tests, we tested data for normality and variance, and differences were considered statistically significant if *P*-values were <0.05 (as in-

dicated with *P <0.05; **P <0.01; ***P <0.001; ns, not significant).

RESULTS

OTULIN maintains GSCs via its de-ubiquitination activity

OTULIN, the linear linkage-specific deubiquitinase, is frequently overexpressed in glioblastoma (Supplementary Figure S1A), and correlates with poor prognosis (Supplementary Figure S1B). We observed that serum-induced GSC differentiation led to loss of expression of OTULIN in different lineages of GSCs (Figure 1A). In contrast, the expression of LUBAC components (HOIP, SHARPIN and HOIL-1L) remained either unchanged or was moderately elevated after differentiation (Supplementary Figure S2A). OTULIN knockdown using lentivirus carrying shRNA substantially impaired GSC self-renewal as assessed by tumor sphere formation (Figure 1B) and *in vitro* limiting dilution assay (Figure 1C), suggesting that OTULIN is indispensable for the maintenance of GSC self-renewal and tumor-initiating ability. Moreover, we found that OTULIN knockdown did not affect the viability of GSCs or induce apoptosis of GSCs (Supplementary Figure S3). Silencing OTULIN inhibited the expression of stem cell-associated transcription factors (e.g. Olig2 and Sox2) in GSCs (as shown later in Supplementary Figure S4), further establishing the essential role of OTULIN for GSC identity and stemness. We constructed a catalytically inactive mutant OTULIN-C129S and a loss-of-binding (to Met1-Ub) mutant OTULIN-W96R (5,7). We found that reconstitution of OTULIN-deficient GSCs with either the OTULIN-C129S or OTULIN-W96R mutant failed to restore the sphere formation and viability of GSCs, in contrast to those with wild-type OTULIN (Figure 1D; Supplementary Figure S2B). These findings together indicated that OTULIN is essential for GSC maintenance and, furthermore, that OTULIN maintains GSC stemness and self-renewal through its enzymatic activity.

Development of a linear Ub probe using genetic code expansion

In order to identify the direct substrates of the deubiquitinase OTULIN, we developed a live cell-compatible linear Ub probe which mimics endogenous Ub and enables enrichment and identification of linear polyUb-modified proteins. Briefly, we introduced a bio-orthogonal reactive residue on lysine-null Ub by encoding a non-canonical amino acid (NAEK) via genetic code expansion. The engineered Ub probe was expressed in target cells. Then a copper-free click-mediated ligation between the azide group on the NAEK-Ub chain and biotin–DIBO was performed, followed by a streptavidin pull-down in almost denaturing conditions (Figure 2A). Proteome-wide substrate identification proceeded with on-bead tryptic digestion and nano liquid chromatography–tandem MS (nanoLC-MS/MS) analysis.

To choose the optimal site for NAEK incorporation, firstly we performed polarity sorting among the surface amino acid residues based on the crystal structure of Ub (PDB entry: 1ubq) and ESFF modeling (see 'Structural modeling' in the Materials and Methods; Supplementary Table S1). We calculated the accessible surface area and the stable energy of Ub variants with NAEK substitution on the candidate sites (Gly10, Lys29, Arg42, Ala46, Arg54 and Asn60) (Figure 2B; Supplementary Table S2). In parallel, we experimentally evaluated the expression efficiency and pull-down efficiency of the Ub variants carrying NAEK on these sites in PylRS/$tRNA_{CUA}$-transduced HEK293T cells. Arg54 was chosen as the insertion site in the following studies because it provides both sufficient expression and effective pull-down (Figure 2C; Supplementary Figure S5) in the described context (see the Materials and Methods). We concomitantly replaced the seven lysine residues on the engineered Ub with arginine. The NAEK-incorporated lysine-null Ub probe (henceforth referred to as NAEK-Ub) thus forms linear chains when conjugated to substrate in cell-free settings (as demonstrated in an *in vitro* ubiquitin chain assembly assay described below; see Figure 2G and H). We ectopically expressed and purified recombinant NAEK-Ub from HEK293T cells (see the Materials and Methods). High resolution MS/MS analysis of the exogenously expressed NAEK-Ub after protease digestion (by trypsin or GluC) confirmed that NAEK was selectively incorporated at the TAG site (Figure 2D). Additionally, NAEK-Ub displayed CD spectra highly similar to those of wild-type Ub, indicating that the secondary and tertiary structures and folding properties of the recombinant NAEK-Ub are identical to those of wild-type Ub (Figure 2E).

We examined the activity of NAEK-Ub using an *in vitro* Ub chain assembly assay (23). We observed that NAEK-Ub could be efficiently recognized by the physiological E2 (i.e. UBE2D3 and UBE2L3) of LUBAC in the presence of UBE1 and ATP (Figure 2F; Supplementary Figure S6). Moreover, NAEK-Ub could be conjugated to the *in vitro* substrate (GST–Ub) by the LUBAC catalytic machinery. The ubiquitination pattern and efficiency of GST–Ub in the presence of NAEK-Ub were identical to those of its wild-type counterpart (Figure 2G). In addition, the linear Ub chain formed by NAEK-Ub was efficiently recognized and hydrolyzed by the linear deubiquitinase OTULIN (Figure 2H; Supplementary Figure S7). These data showed that NAEK-Ub is compatible with the linear ubiquitination machinery *in vitro*.

Next we tested the cell compatibility of the orthogonal translation system, the *Methanosarcina barkeri* MS pyrrolysyl tRNA synthetase/$tRNA_{CUA}$ pair (MbpylRS/$tRNA_{CUA}$) (24), which was applied to GSCs for the first time. For optimal delivery, we transduced the patient-derived GSC line (GSC456) with lentiviral vectors for integration of genes encoding PylRS/$tRNA_{CUA}$ cassettes and an amber codon-containing ubiquitin (Ub-54TAG) into the host genome, respectively (Supplementary Figure S8A, B). We used the EF-1 promoter to drive PylRS and NAEK-Ub expression as this promoter afforded superior expression in undifferentiated stem cells (25,26). The resultant GSCs were supplemented with 1 mM NAEK for 24 h, and then subjected to reaction with biotin–DIBO via a copper-free click ligation [also termed SPAAC (27)] (Figure 2A). The subsequent streptavidin pull-down demonstrated that the engineered Ub bait was readily expressed in GSCs in the presence of NAEK. No Ub

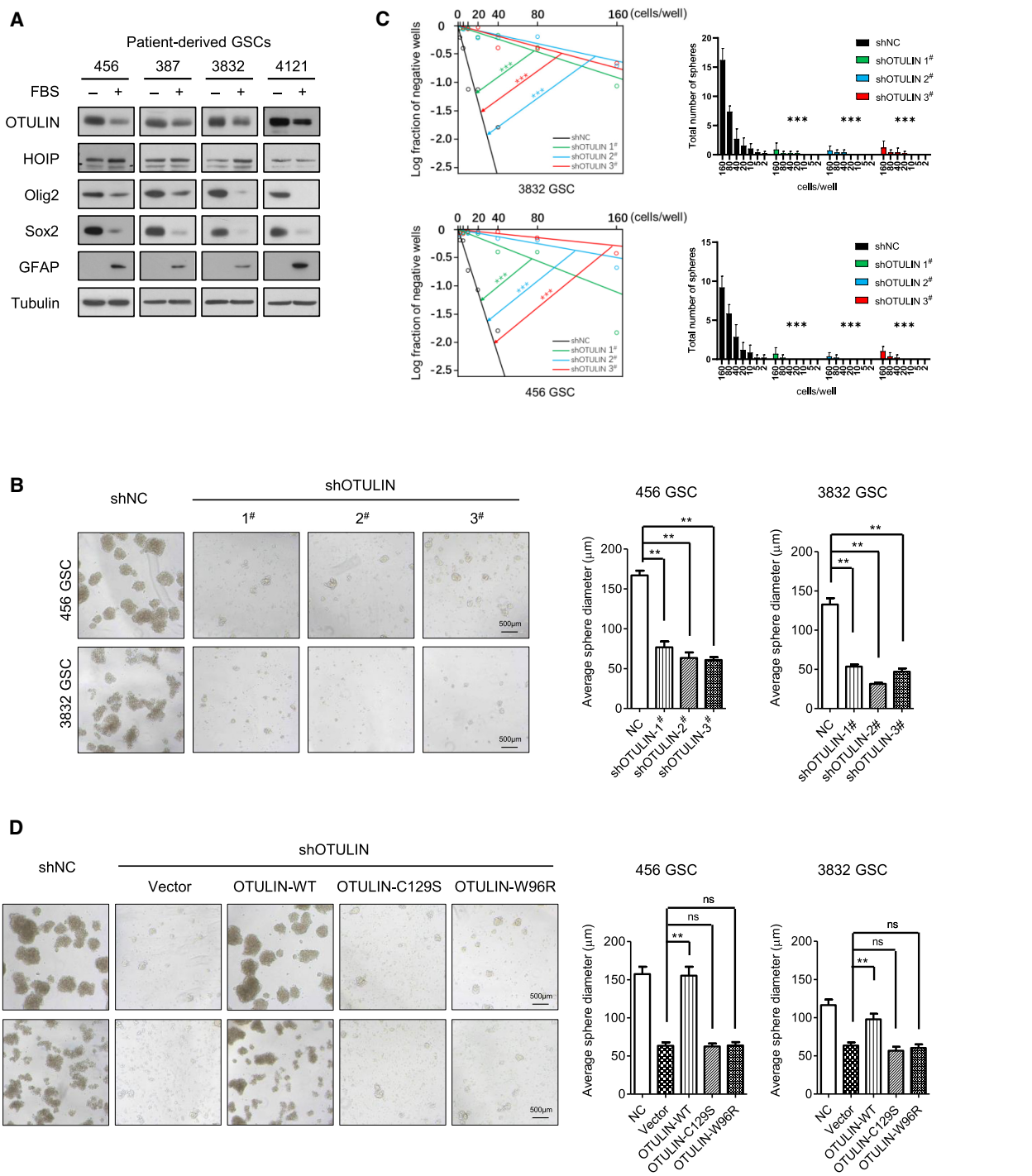

Figure 1. OTULIN maintains GSCs via its de-ubiquitination activity. (**A**) Immunoblot analysis of OTULIN, HOIP, the GSC markers (Olig2 and Sox2) and the differentiation marker (GFAP) in GSCs isolated from four glioblastoma tumors before and after serum-induced GSC differentiation. (**B**) Effects of OTULIN knockdown with three different shRNA sequences on tumor sphere formation of GSCs. Representative images (phase contrast) of tumor spheres are shown (scale bar, 500 μm). Quantification shows that OTULIN knockdown significantly reduced GSC tumor sphere size. (**C**) *In vitro* limiting dilution assays of GSCs transduced with shNC or shOTULIN. GSCs were plated into 96-well plates at various seeding densities (2–160 cells per well). Each well was evaluated for the presence or absence of tumor spheres after differentiation. Limiting dilution analysis was performed using online software (http://bioinf.wehi.edu.au/software/elda/). The total numbers of tumor spheres per well are presented as means ± SD of three independent measurements. Statistical significance of sphere numbers was determined by one-way ANOVA with Tukey's multiple comparison. ***P <0.001. (**D**) Tumor sphere formation of GSCs transduced with flag-OTULIN-wild type, flag-OTULIN-C129S, flag-OTULIN-W96R and vector control in combination with shOTULIN or shNC control. The expression efficiency is shown in Supplementary Figure S2B. Representative images of tumor spheres are shown (scale bar, 500 μm). Quantification shows that ectopic expression of inactive OTULIN mutants (C129S and W96R) in GSCs cannot rescue the impaired tumor sphere formation and the decreased tumor sphere size. Quantitative data are presented as means ± SD of three independent measurements. ns, not significant, **P <0.01.

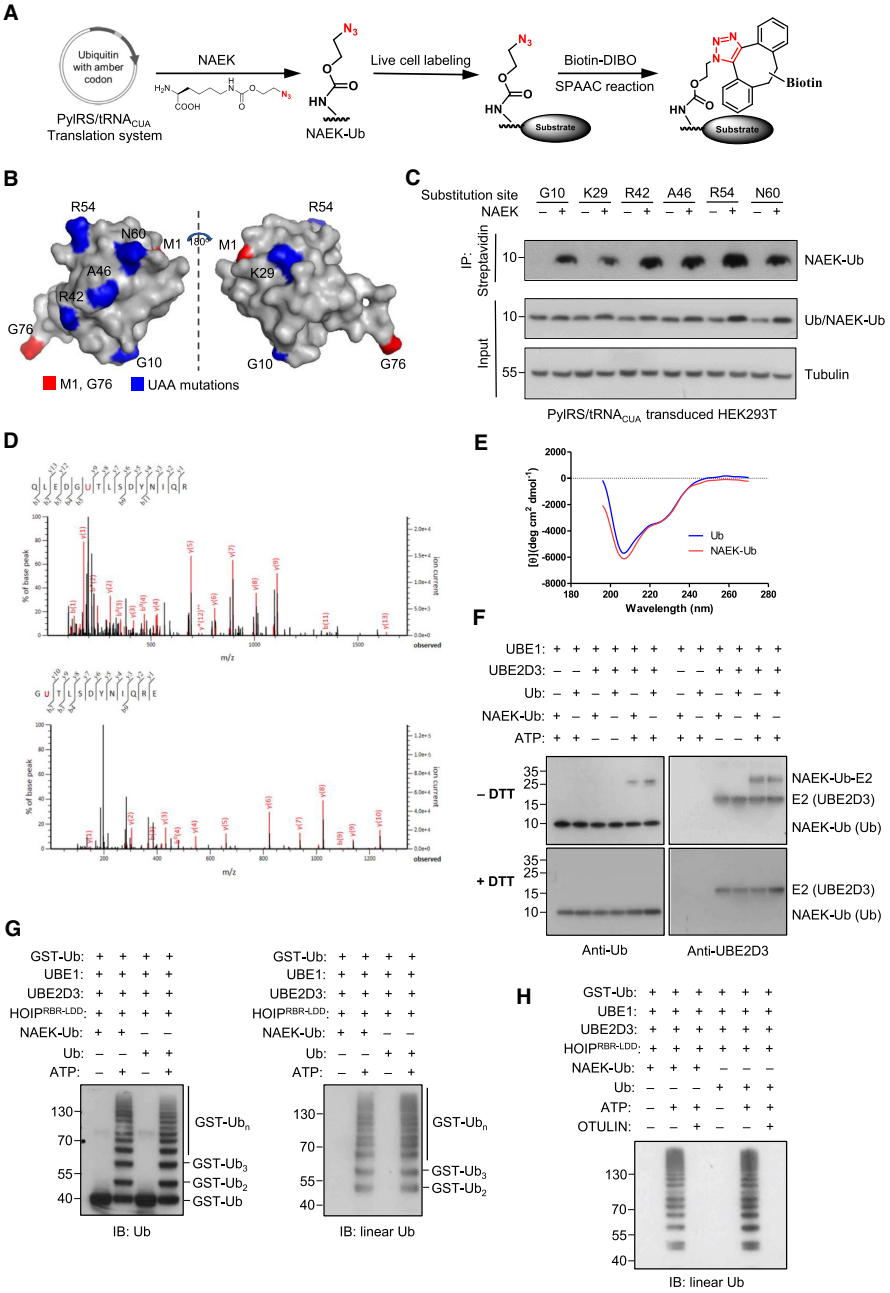

Figure 2. The development and evaluation of the NAEK-Ub probe. (**A**) The scheme of the bio-orthogonal NAEK-Ub strategy. GSCs were transduced with a modified pCDH lentivector for integration of the genes encoding PylRS/tRNA$_{CUA}$ expression cassettes and an amber codon-containing ubiquitin (Ub-54TAG) into the host genome. The resultant transgenic cells, GSC-tRNA/pylRS/Ub-54TAG, were then supplemented with NAEK for 24 h, producing NAEK-Ub which readily conjugates to the substrates of linear Ub. The SPAAC reaction between the azides of the NAEK-Ub chain and biotin–DIBO facilitates enrichment and identification of the linear Ub-modified proteins. (**B**) Ub structure labeled with the surface residues (in blue) and the terminal residues (in red) (generated by PyMOL). The accessible surface area and the stable energy of Ub variants with NAEK substitution on each candidate site (Gly10, Lys29, Arg42, Ala46, Arg54 and Asn60) are shown in Supplementary Table S2. (**C**) The expression and pull-down efficiency of Ub variants with NAEK incorporated at different sites (Gly10, Lys29, Arg42, Ala46, Arg54 and Aln60) in PylRS/tRNA$_{CUA}$-transduced HEK293T cells. Arg54 was finally chosen as the insertion site for NAEK. (**D**) High resolution tandem MS identification of NAEK-Ub peptides after protease digestion. A representative MS/MS fragment spectrum of the characteristic peptide QLEDGU^{54}TLSDYNIQR (by trypsin) is shown. The NAEK insertion site was further confirmed by the GluC-digested peptide GU^{54}TLSDYNIQRE. **U** (in red) represents NAEK. (**E**) CD spectra of wild-type ubiquitin (blue curve) and NAEK-Ub (red curve) in 50 mM sodium phosphate buffer (pH 7.4). (**F**) Wild-type Ub and NAEK-Ub were reacted with the E2 enzyme UBE2D3 in the presence of UBE1 and ATP. The conjugation of Ub and NAEK-Ub onto the E2 via thioester bonds in the reactions was analyzed by SDS–PAGE with or without DTT. (**G**) *In vitro* ubiquitin chain assembly assay of wild-type Ub and NAEK-Ub. Ub or NAEK-Ub was incubated with the linear ubiquitination machinery (composed of UBE1, UBE2D3 and HOIP$^{RBR-LDD}$) and recombinant GST–Ub (acceptor ubiquitin) in the presence or absence of ATP. The ladders of polyUb chains are assessed by immunoblotting using anti-Ub antibody (left) and anti-linear Ub antibody (right), respectively. Standard reaction conditions are described in the Materials and Methods. (**H**) The polyUb chains of wild-type Ub and NAEK-Ub were prepared as described in (G). The resultant reactions were incubated with 0.2 μg/ml OTULIN at 37°C for 1 h. Immunoblotting was performed with anti-linear Ub antibody. The corresponding silver-stained gel is shown in Supplementary Figure S4.

signal was observed in the control sample without NAEK, demonstrating the high specificity of the labeling and pull-down process. We separately constructed an engineered green fluorescent protein (GFP-39TAG) to benchmark the procedure. Robust GFP fluorescence was only observed in the NAEK-supplemented group (Supplementary Figure S8C), further confirming the feasibility and specificity of the PylRS/$tRNA_{CUA}$ translation system in GSCs. Taken together, these results demonstrated that the optimized orthogonal translation system is able to site specifically incorporate NAEK into proteins (i.e. Ub) in response to the TAG codon in the target GSC context.

Global profiling of linear Ub substrates in live cells with the NAEK-Ub strategy

We envisage that the engineered 'linear Ub bait' (NAEK-Ub) integrates the advantages of genetic encoding to achieve live cell compatibility, and of click-mediated ligation to achieve bio-orthogonal reactivity and label specificity. The covalent linkage and stringent clean up minimize the false positives resulting from non-covalent binding, and therefore provide specific enrichment and identification of the bona fide substrates. This is particularly beneficial to low-abundance linear Ub substrates such as transcription factors. Moreover, the NAEK-Ub probe was chemically inducible and expressed only upon NAEK spiking. The expression of NAEK-Ub was maintained at an appropriate level that did not perturb normal cellular functions (i.e. NF-κB signaling, as shown in Supplementary Figure S9). As a proof-of-concept, we coupled NAEK-Ub pull-down with MS analysis, and applied this pipeline to a cellular model of tumor necrosis factor α (TNFα)-induced inflammation. HEK293T cells transduced with PylRS/$tRNA_{CUA}$/Ub-54TAG were starved overnight and then treated with TNFα for 15 min (Figure 3A). The increased level of phosphorylated p65 indicated the activation of the NF-κB pathway (Figure 3B). After removing the TNFα, the resultant cells were treated with NAEK for 24 h, followed by a copper-free click reaction and biotin–streptavidin pull-down (Figure 3A). The subsequent high-resolution MS analysis identified most of the known substrates of linear ubiquitination in at least two out of three biological replicates (Figure 3C; Supplementary Table S3), including the well characterized substrates NEMO (9,28), RNF31 (29), RIPK1 (4), TRIM25 (30), FADD (31), STAT1 (12) and AGO2 (32). Label-free proteomics quantification (by MaxQuant, data quality control shown in Supplementary Figure S10) revealed 623 significantly up-regulated proteins in the TNFα-stimulated group compared with the control (Figure 3C, D; Supplementary Table S4, with the criteria of P-value <0.05 and fold change >1.5). NEMO was ranked as one of the most enriched proteins as expected, gauging the feasibility of the workflow (Figure 3C). Gene Ontology analysis of the enriched proteins highlights the role of linear ubiquitination in NF-κB signaling (Figure 3E). The enriched pathways covered the previously established functions of linear ubiquitination [i.e. bacterial and viral infections (33,34), viral-induced pro-inflammatory response (35,36), proteasome- and Ub-mediated proteolysis (37) and protein quality control (38) (Figure 3E)]. In addition, the association of linear ubiquitination with mitosis and the cell cycle has been demonstrated by our previous work (13). The emerging role of linear ubiquitination in mRNA homeostasis has also been described in a recent publication (32). We further validated several highly enriched proteins (e.g. RDH10, SLC30A7 and ZNFR2) as putative linear Ub substrates using a cellular ubiquitination assay (13). The specificity of the linear polyUb-specific antibody (1F11/3F5/Y102L) has been demonstrated previously (14). We observed intense linear polyUb signals on these proteins when co-expressed with LUBAC in HEK293T cells (Figure 3F; Supplementary Figure S14). These results together demonstrated that NAEK-Ub functions well in living cells and allows enrichment and identification of linear polyUb-modified proteins.

Identification of STAT3 as a bona fide substrate of linear Ub in GSCs

Next we implemented the bio-orthogonal strategy described above for the profiling of linear Ub-modified proteins in GSCs. The PylRS/$tRNA_{CUA}$/Ub-54TAG transgenic GSCs were infected with lentivirus carrying shOTULIN or shNC, respectively, as described. The resultant cells were treated with NAEK for 24 h, followed by a copper-free click reaction and biotin–streptavidin pull-down (Figure 4A). We achieved a clear knockdown of OTULIN with shRNA, and observed a significant elevation of the total linear ubiquitination in shOTULIN GSCs (Figure 4B). A total of 2701 proteins were identified by MS in at least two independent biological replicates (Figure 4C; Supplementary Table S5), including the known substrates [as benchmark control, i.e. NEMO (9), TRAF6 (16), STAT1 (12), etc.]. Quantitative analysis of the NAEK-Ub pull-down proteome revealed that the essential transcription activator STAT3 was significantly enriched in OTULIN knockdown groups in comparison with the controls (Figure 4C; Supplementary Table S6). This observation inspired us to explore the functional relevance between linear ubiquitination and STAT3 signaling in GSCs.

We confirmed that STAT3 could be readily linearly ubiquitinated by co-transfection of LUBAC in HEK293T cells using NEMO as an experimental control (Figure 4D). The linear ubiquitination of STAT3 was abolished by co-expression of $OTULIN^{WT}$, but not catalytically inactive $OTULIN^{C129S}$ (Figure 4E). These results were supported by the *in vitro* ubiquitination assay which showed that the linear Ub chain of STAT3 was formed by LUBAC and removed by OTULIN (Figure 4F). We further examined the linear ubiquitination of endogenous STAT3 in GSCs. Immunoprecipitation of endogenous STAT3 revealed that while linear ubiquitination of STAT3 was maintained at a relatively low level in undifferentiated GSCs, it increased significantly in response to OTULIN depletion (Figure 4G). This is in line with the NAEK-Ub proteomics data, and confirms that STAT3 is a bona fide substrate of linear Ub.

Characterization of linear Ub sites on STAT3

We mapped the linear ubiquitination sites of STAT3 with high-resolution MS. We identified four lysine residues as potential sites of linear ubiquitination, which were all located

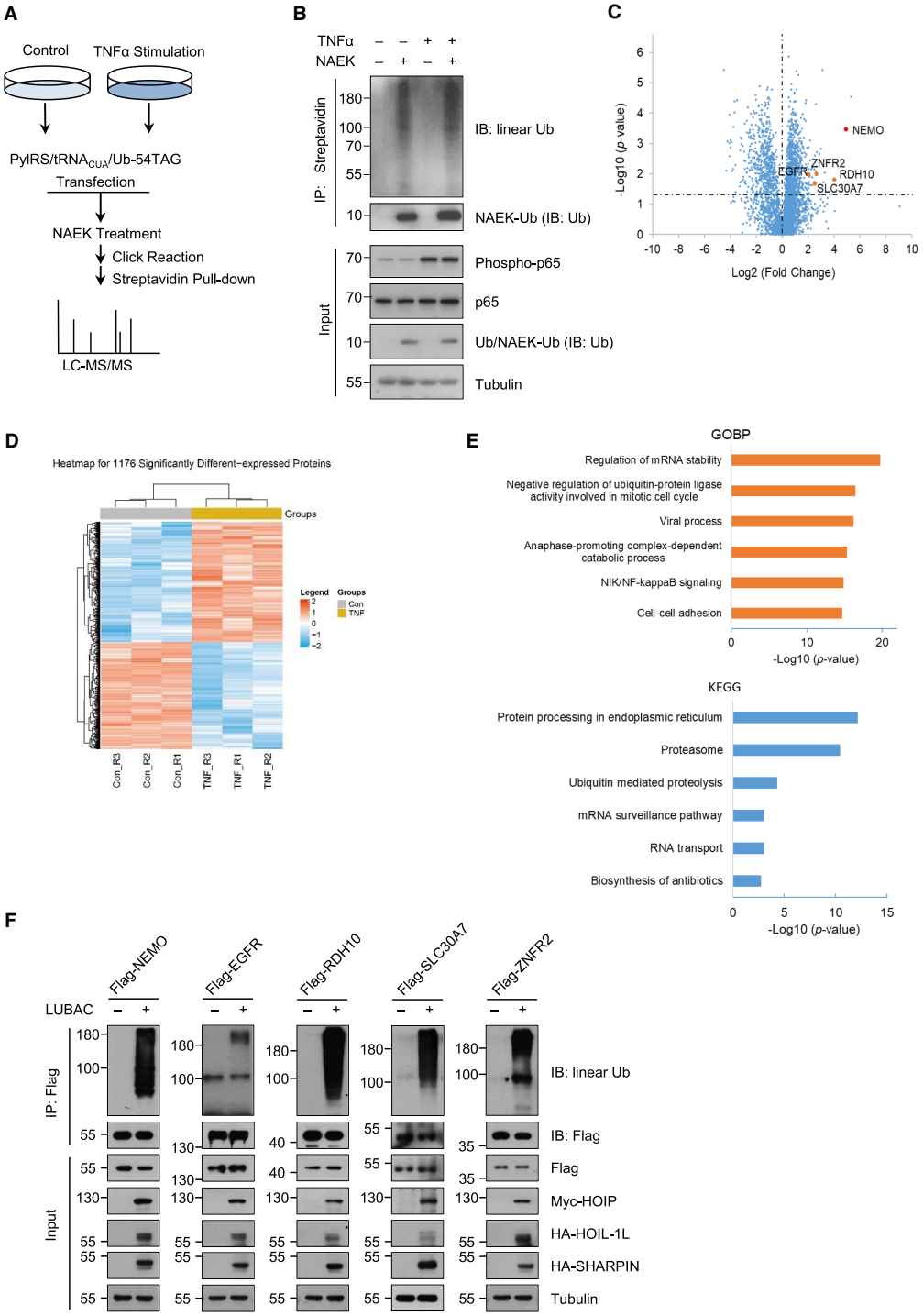

Figure 3. Global profiling of linear Ub substrates in live cells with NAEK-Ub. (**A**) Schematic workflow of NAEK-Ub proteomics. HEK293T cells were transfected with plasmids of the PylRS/tRNA$_{CUA}$ pair and Ub-54TAG, and were cultured in DMEM supplemented with 1 mM NAEK for 24 h. The resultant cells were serum starved overnight and then treated with TNFα (10 ng/μl) for 15 min. Cell lysates were incubated with biotin–DIBO (10 μM) at room temperature for 2 h and then immunoprecipitated with streptavidin beads. The enriched proteins were digested by trypsin and subjected to LC-MS/MS analysis. (**B**) HEK293T cells transduced with PylRS/tRNA$_{CUA}$/Ub-54TAG were starved overnight and then treated with TNFα for 15 min. Phosphorylated p65 indicates the activation of NF-κB. The streptavidin pull-down fraction was immunoblotted against anti-linear Ub. (**C**) Differential analysis of NAEK-Ub pull-downs (visualized by volcano plot; source data shown in Supplementary Table S3) in the TNFα-treated group and the control. The previously reported substrate NEMO was labeled in red as a benchmark. Putative substrates selected for further validation were labeled in orange. (**D**) Hierarchical clustering of differential proteins derived from NAEK-Ub pull-downs between the TNFα-treated group and the control group (source data shown in Supplementary Table S4). (**E**) Pathway analysis and annotation of proteins enriched in the TNFα-treated group by Gene Ontology Biological Processes (GOBP) and Kyoto Encyclopaedia of Genes and Genomes (KEGG). (**F**) Verification of putative linear Ub substrates. The plasmid of each Flag-tagged candidate protein was transfected into HEK293T cells with or without LUBAC components (Myc-HOIP, HA-HOIL-1L and HA-SHARPIN). Immunoprecipitation was performed with anti-Flag M2 beads. Flag-NEMO was used as a system control.

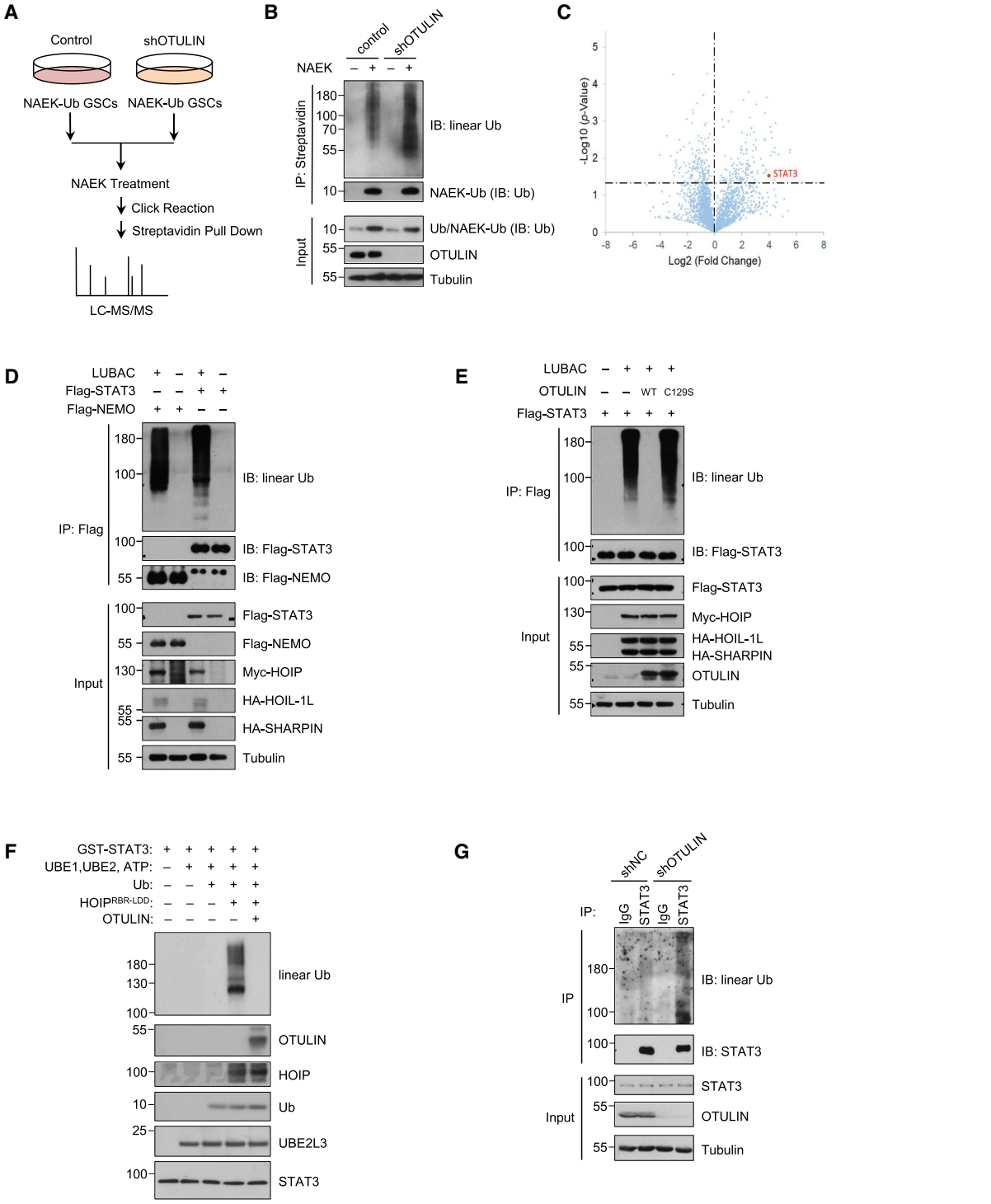

Figure 4. STAT3 is a direct substrate of linear Ub. (**A**) Workflow of NAEK-Ub proteomics to identify linear Ub-modified proteins in OTULIN-depleted GSCs. (**B**) Immunoblot analysis of NAEK-Ub pull-downs in shOTULIN GSCs and the control. OTULIN depletion leads to an overall increase of linear Ub signals. (**C**) Volcano plot of the quantitative comparison of the NAEK-Ub proteome in shOTULIN GSCs and the controls (source data are shown in Supplementary Table S5). STAT3 (labeled in orange) is selected for subsequent validation and functional evaluation. (**D**) Immunoprecipitation (IP) analysis of linear ubiquitination of STAT3 in HEK293T cells co-transfected with LUBAC (comprising Myc-HOIP, HA-HOIL-1L and HA-Sharpin). IP was performed with anti-Flag M2 beads. Flag-NEMO was used as a system control. (**E**) IP analysis of linear ubiquitination of STAT3 in HEK293T cells co-transfected with LUBAC, together with either wild-type OTULIN or its catalytically inactive mutant (OTULIN^{C129S}). STAT3 IP was performed with anti-Flag M2 beads. (**F**) *In vitro* linear ubiquitination assay of GST–STAT3 with or without OTULIN. Recombinant GST–STAT3 was incubated with the linear ubiquitination machinery (composed of UBE1, UBE2D3, HOIPRBR-LDD and Ub) with or without OTULIN. The reaction was carried out at 37°C for 2 h and analyzed by immunoblotting. (**G**) IP analysis of linear ubiquitination of endogenous STAT3 in undifferentiated GSCs transduced with either lentiviral shOTULIN or shNC. IP of endogenous STAT3 was performed using anti-STAT3 antibody, and was immunoblotted with anti-linear Ub antibody.

at the coiled-coil domain of STAT3 (K153, K161, K163 and K199). Those sites are conserved in vertebrates (Figure 5A). The mass spectra of the identified ubiquitinated peptides of STAT3 and the characteristic linear Ub peptide (GGMQIFVK) are shown in Figure 5B. We mutated the four lysine residues of STAT3 to arginine and examined the linear ubiquitination status of the mutants. While single site mutation partially reduced the intensity of linear ubiquitination on STAT3, simultaneous mutation of four sites (4KR) substantially abolished the linear ubiquitination signals of STAT3 (Figure 5C). These data suggested that the identified sites (K153, K161, K163 and K199) are the dominant linear ubiquitination sites of STAT3.

To evaluate the functional significance of linear ubiquitination on STAT3, we exogenously expressed wild-type STAT3 or the STAT3-4KR mutant in a STAT3-null cell line [STAT3(–/–) HeLa cell]. We observed that ectopic expression of the STAT3-4KR mutant dramatically enhanced the IL-6-induced STAT3 phosphorylation (Y705p) and increased downstream transcription (e.g. SOCS3 and c-MYC) compared with the wild-type counterpart (Figure 5D, E). This result demonstrated that STAT3-4KR is a gain-of-function mutant. Linear ubiquitination may serve as a negative regulator of STAT3 that impedes STAT3 activation.

OTULIN maintains persistent activation of STAT3 in GSCs

GSCs show constitutively active STAT3 signaling (21,39), evidenced by a high basal level of tyrosine-phosphorylated STAT3 (Supplementary Figure S4). Lentivirus-mediated OTULIN knockdown greatly attenuated the basal phosphorylation of STAT3, and impaired the transcription of STAT3 in GSCs (Supplementary Figure S4). Such an impairment was also observed for GSC transcriptional factors Olig2 and Sox2 (to a lesser extent), whose expression was promoted by STAT3 (21) (Supplementary Figure S4). In the context of IL-6 stimulation, OTULIN knockdown considerably reduced the level of STAT3 tyrosine phosphorylation (Figure 6A), thereby preventing the nuclear translocation of STAT3 (Figure 6B). These data supported that OTULIN directly regulates STAT3 signaling in GSCs.

To interrogate whether the regulation by OTULIN of STAT3 activity was mediated by the linear Ub sites of STAT3, we transduced the lentiviral shRNA-resistant flag-tagged STAT3-WT or STAT3-4KR mutant to GSCs and depleted endogenous STAT3 in GSCs by lentiviral shRNA. We examined the expression of the activated form of STAT3 (STAT3-Y705p) and measured the transcription of STAT3 target genes. We found that upon IL-6 stimulation, the non-linear-ubiquitinated mutant (STAT3-4KR), rather than the wild-type counterpart, restored the impaired phosphorylation and transcription signaling of STAT3 caused by silencing OTULIN (Figure 6C, D). Moreover, the STAT3-4KR mutant reversed the inhibitory effect of OTULIN knockdown on STAT3 nuclear translocation in response to IL-6 treatment (Figure 6E). The loss of the GSC stem cell-like phenotype and growth suppression induced by OTULIN depletion was also substantially rescued, as supported by the restoration of tumor sphere formation in STAT3-4KR-expressing GSCs (Figure 6F). Taken together, these data indicated that the accumulated linear ubiquitination on STAT3 caused by OTULIN knockdown is an intrinsic inhibitory mechanism against its phosphorylation and transcriptional activity. OTULIN promotes persistent STAT3 activation via restricting linear ubiquitination of STAT3, and therefore maintains the stemness and self-renewal of GSCs.

Linear ubiquitination impairs STAT3 activation by recruiting its phosphatase TC-PTP

We further explored how STAT3 linear ubiquitination blocks its activation in GSCs. We found that treatment of GSCs with the tyrosine phosphatase inhibitor pervanadate largely reversed the attenuation of STAT3 phosphorylation induced by OTULIN knockdown (Figure 7A), suggesting that the phosphatase of STAT3 may be involved in the inhibitory effect of STAT3 linear ubiquitination on its phosphorylation. The nuclear isoform of TC-PTP is reported to be responsible for STAT3 dephosphorylation (40,41). Immunoprecipitation of endogenous STAT3 from GSCs revealed that the interaction between TC-PTP and STAT3 was readily detectable in response to IL-6 treatment, which is consistent with previous reports (42). We observed that OTULIN knockdown greatly enhanced the interaction between TC-PTP and STAT3 in GSCs, whereas it showed no impact on STAT3 binding with JAK2 (Figure 7B). Moreover, we found that the linear Ub-null mutation (STAT3-4KR) profoundly impaired the interaction between STAT3 and TC-PTP induced by IL-6, whereas the binding of JAK2 with STAT3-4KR was not affected (Figure 7C). Taken together, the above data supported a model whereby instead of directly inhibiting JAK2-induced STAT3 activation, linear ubiquitination of STAT3 promotes the recruitment of TC-PTP to activated STAT3, thereby resulting in STAT3 dephosphorylation and inactivation (Figure 7D).

DISCUSSION

Global profiling of linear Ub substrates represents a significant challenge because of the low cellular abundance, the non-specific binding and the linkage dynamics. Here we report an application of genetic code expansion, which couples the UAA-mediated blank codon suppression with the Ub chain assembly process, to the development of a linear Ub affinity probe NAEK-Ub. In comparison with conventional methods, our NAEK-Ub strategy offers unique advantages. First, the genetically tagged NAEK-Ub minimizes perturbation of the native Ub structure and linkage capability, and is compatible with the endogenous linear Ub machinery. Second, the bio-orthogonal reaction is accomplished in a live cell context, and is thus expected to be of more physiological relevance. Third, the covalent tagging allows pull-down of the bona fide substrates of linear Ub in nearly denaturing conditions. The tolerance of stringent washing restricts most interference arising from non-specific binding. Overall, the engineered probe NAEK-Ub is compatible with live cells, able to capture and covalently lock linear Ub proteins and directly enriches the linear Ub-modified proteins for sensitive detection. As a proof-of-concept, we applied this strategy to patient-derived GSCs, an aggressive subset of cancer cells which drive

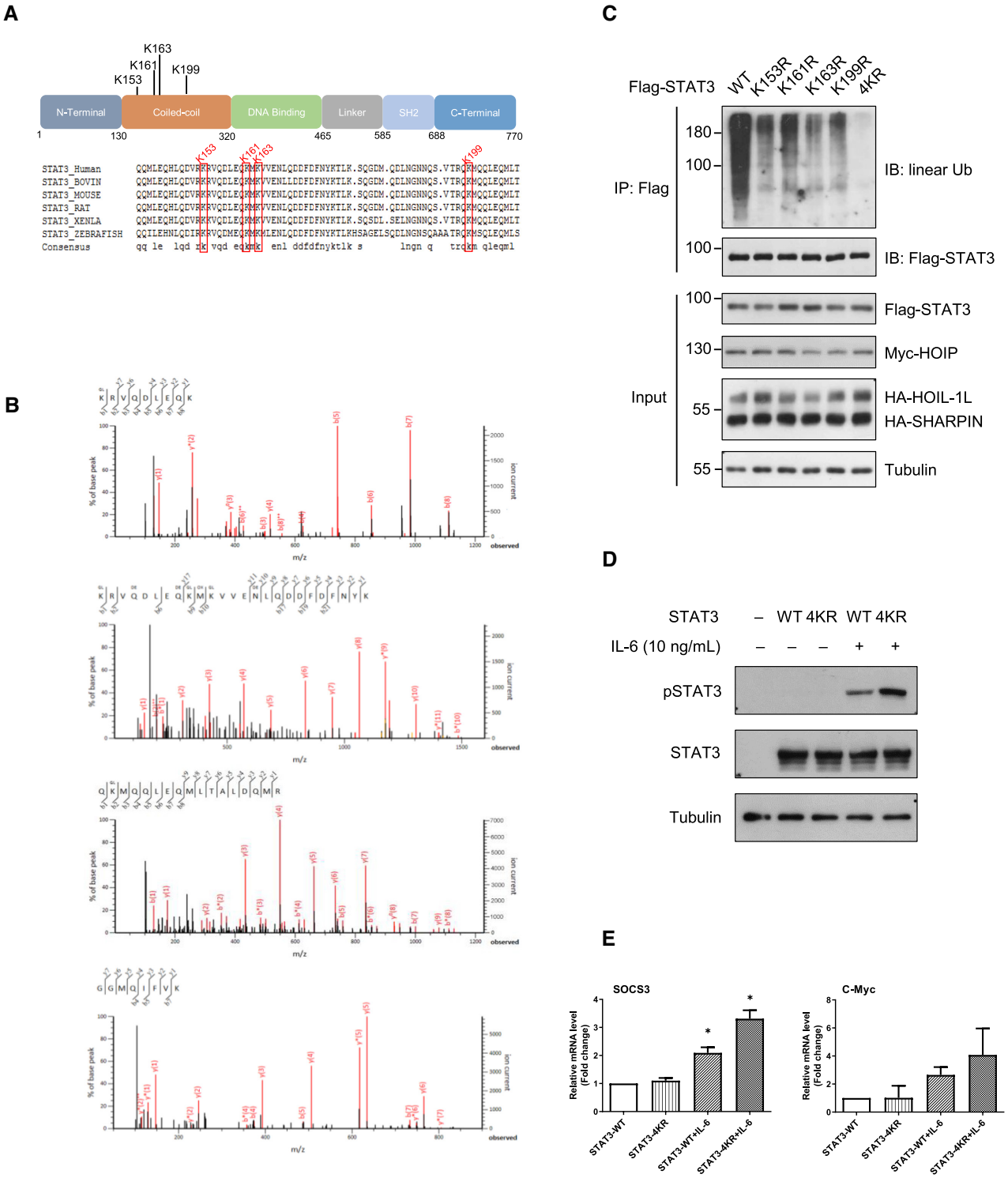

Figure 5. Identification of linear Ub sites on STAT3. (**A**) The identified linear ubiquitination sites of STAT3 (Lys153, Lys161, Lys163 and Lys191) and their evolutionary conservation in vertebrates. K refers to a lysine residue. (**B**) Representative MS/MS spectra of linear ubiquitinated peptides of STAT3 (with linear Ub sites identified at Lys153, Lys161, Lys163 and Lys191), and the MS/MS spectrum of the characteristic linear Ub peptide (GGMQIFVK) generated by trypsin digestion (shown at the bottom). (**C**) IP analysis of linear ubiquitination of STAT3 in HEK293T cells transfected, respectively, with wild-type STAT3, STAT3-K153R, STAT3-K161R, STAT3-K163R, STAT3-K199R or STAT3-4KR (STAT3-K153/161/163/199R) mutants, and co-transfected with LUBAC. (**D**) STAT3(–/–) HeLa cells were transduced with wild-type STAT3 or the STAT3-4KR mutant, followed by treatment with 10 ng/ml IL-6 for 1 h. Immunoblot analysis of pY705-STAT3 and total STAT3 was performed. (**E**) qPCR analysis of the STAT3-targeted genes SOCS3 and c-Myc in STAT3(–/–) HeLa cells transduced with wild-type STAT3 or the STAT3-4KR mutant after IL-6 treatment (10 ng/ml). Data are presented as the mean ± SD, $n = 3$, *$P < 0.05$, Student's t-test.

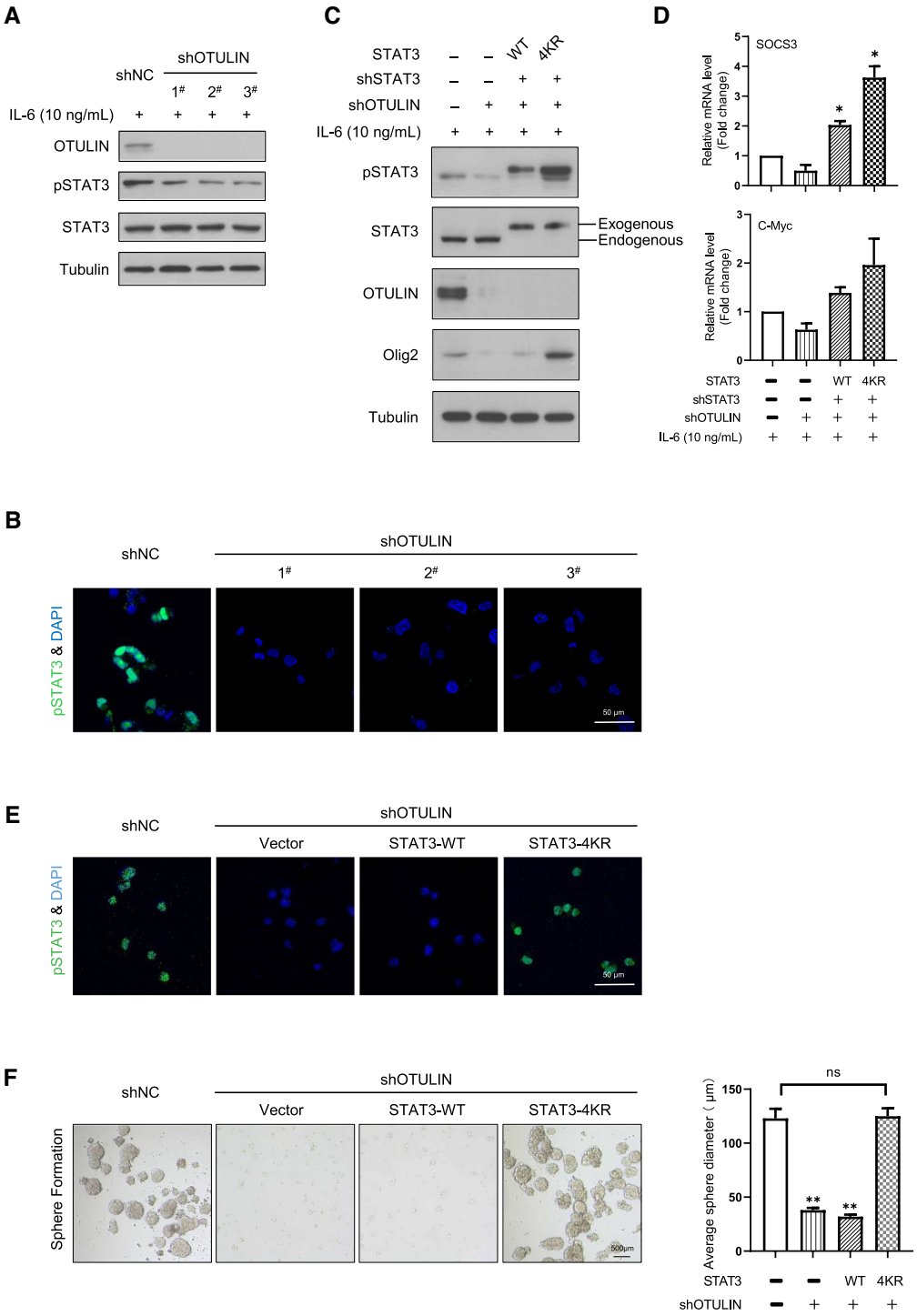

Figure 6. OTULIN regulates STAT3 signaling in GSCs. (**A**) GSCs were transduced with lentiviral shOTULIN or shNC, and treated with 10 ng/ml IL-6 for 30 min. pY705-STAT3 and total STAT3 were analyzed by immunoblotting. (**B**) Immunofluorescence (IF) staining of pY705-STAT3 (green) on GSCs transduced with lentiviral shOTULIN or shNC. The GSCs were pre-treated with IL-6 (10 ng/ml) for 30 min. DAPI (blue) was used to stain nuclei. Scale bar, 50 μm. (**C**) Immunoblots of pY705-STAT3, STAT3 and Olig2 in GSCs transduced with lentiviral shOTULIN or shNC. The endogenous STAT3 in GSCs was replaced by the lentiviral shRNA-resistant flag-tagged STAT3 wild type (WT) or STAT3-4KR mutant. The GSCs were treated with IL-6 (10 ng/ml) for 30 min before cell lysis. (**D**) qPCR analysis of the STAT3-targeted genes SOCS3 and c-Myc in the same batch of GSC samples as described in (C)**.** Data are presented as the mean ± SD ($n = 3$). *P <0.05. (**E**) IF staining of pY705-STAT3 (green) on GSCs, and GSCs expressing the wild-type STAT3 or STAT3-4KR mutant, in combination with lentiviral shOTULIN or shNC. The GSCs were pre-treated with IL-6 (10 ng/ml) for 30 min. DAPI (blue) was used to stain nuclei. Scale bar, 50 μm. (**F**) Tumor sphere formation of GSCs transduced with lentiviral shOTULIN or shNC. The endogenous STAT3 in GSCs was replaced by the lentiviral shRNA-resistant flag-tagged STAT3 WT or STAT3-4KR mutant. Representative images of tumor spheres are shown (scale bar, 500 μm). Quantification shows that reconstitution of the STAT3-4KR mutant in GSCs rescued the decreased tumor sphere size caused by OTULIN depletion. Quantitative data are presented as the means ± SD of three independent measurements. ns, not significant; **P <0.01.

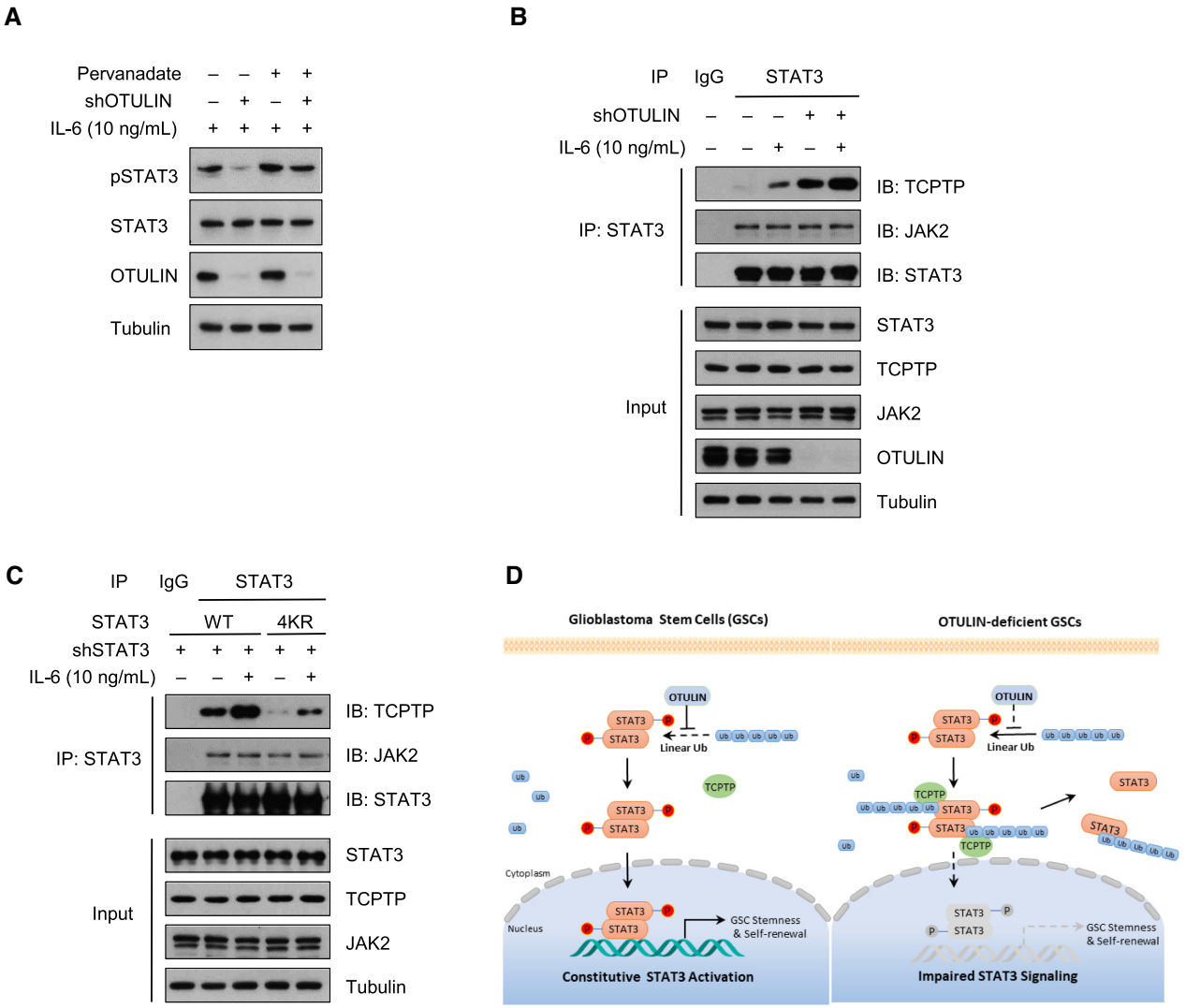

Figure 7. Linear ubiquitination impairs STAT3 activation. (**A**) GSCs were transduced with lentiviral shOTULIN or shNC, and were pre-treated or not with pervanadate (50 μM) for 6 h, followed by IL-6 (10 ng/ml) stimulation for 30 min. pY705-STAT3 and total STAT3 were analyzed by immunoblotting. (**B**) GSCs transduced with either lentiviral shNC or shOTULIN, and followed by IL-6 (10 ng/ml) treatment for 30 min. GSCs were lysed and immunoprecipitated with either control IgG or anti-STAT3 antibody. The IP samples and input (5%) were immunoblotted with TC-PTP and JAK2. (**C**) The endogenous STAT3 in GSCs was replaced by lentiviral shRNA-resistant Flag-tagged STAT3 WT or STAT3-4KR mutant, and followed by IL-6 (10 ng/ml) treatment for 30 min. GSCs were lysed and immunoprecipitated with either control IgG or anti-STAT3 antibody as indicated. The IP samples and input (5%) were immunoblotted with anti-TC-PTP antibody and anti-JAK2 antibody. (**D**) The proposed working model. Linear ubiquitination impairs STAT3 activity by recruitment of the phosphatase TC-PTP to STAT3 (right panel). OTULIN restricts linear ubiquitination on STAT3, drives persistent STAT3 signaling and therefore maintains the stemness and self-renewal of GSCs (left panel).

malignancy and therapeutic resistance of glioblastoma. The resultant dataset provides a proteome-wide determination of the substrates of linear ubiquitination in a living system, and expands the range of linear ubiquitination substrates.

With NAEK-Ub-based chemical proteomics, we identified STAT3 as a direct substrate of linear Ub in GSCs. Unlike previously reported substrates (e.g. NEMO, RIPK and TRAF6) of which the linear Ub modification remains low in the quiescent state and is inducible upon specific stimuli (e.g. lipopolysaccharide or TNFα), linear ubiquitination of STAT3 is deubiquitinase dependent in the context of undifferentiated GSCs. The endogenous level of linear Ub on STAT3 was substantially increased upon OTULIN knockdown, indicating that STAT3 linear ubiquitination is directly regulated by OTULIN in GSCs.

STAT3 is an essential transcriptional factor that drives cell survival, proliferation and differentiation (43). In normal cells, STAT3 activation is usually transient and tightly regulated. However, in a malignant subset such as GSCs, STAT3 remains persistently activated, leading to the stem cell-like phenotype (i.e. high capacity for self-renewal and chemotherapy resistance)(21,39). The underlying mechanism by which STAT3 is kept persistently activated in GSCs remains a long-standing question. Whereas multiple post-translational modifications [e.g. tyrosine phosphorylation (44), lysine methylation (45) and cysteine palmitoylation (46)] have been reported to promote STAT3 activation,

the negative regulation of STAT3 signaling has remained largely elusive. Clearly, constitutive activation of STAT3, which contributes to the malignancy of glioblastoma, occurs when negative regulation is not fully effective. We identified linear ubiquitination of STAT3 as an intrinsic inhibitory mechanism against its phosphorylation and transcriptional activity in GSCs. Consistently, we observed that the linear Ub-specific deubiquitinase OTULIN is preferentially expressed in undifferentiated GSCs. We demonstrated that the high expression of OTULIN in GSCs restricts linear ubiquitination on STAT3, drives persistent STAT3 signaling and therefore maintains the stemness and self-renewal of GSCs. Our finding reveals an essential link between linear ubiquitination and aberrant STAT3 signaling in GSCs, and suggests that the OTULIN–STAT3 axis could be a potential therapeutic target for malignant cancers such as glioblastoma. This knowledge will facilitate new therapeutic approaches towards diseases associated with overactivated STAT3 signaling.

Given the fact that Ub depletion is lethal and would substantially perturb the cellular network, we performed NAEK-Ub proteomic studies in the presence of endogenous Ub. In addition to forming homotypic linear ubiquitin chains, NAEK-Ub can also conjugate to and linearly extend pre-existing Ub chains in the presence of LUBAC, resulting in mixed polyUb chains. In our experiments, we carefully examined the NAEK-Ub pull-downs using immunoblotting against the general Ub antibody and Ub linkage-specific antibodies (e.g. anti-linear Ub-, anti-K48 polyUb- and anti-K63 polyUb-), respectively. The results showed that NAEK-Ub predominantly forms linear chains rather than other Ub topologies in our experimental settings (see Supplementary Figures S11 and S12). This conclusion was supported by the Ub chain restriction assay (47), in which the NAEK-Ub pull-downs were further incubated with the linear linkage-specific deubiquitinase OTULIN *in vitro*, followed by immunoblotting (see Supplementary Figure S13) and MS-based analysis. The possible false positives can be further eliminated in the proteomic comparison by setting an additional group following *in vitro* OTULIN treatment. Nevertheless, we did not completely exclude the possibility of the formation of mixed linkages in our candidate list. We distinguished the linkage type of those candidates in immunoblotting using Ub linkage-specific antibodies (as shown in Supplementary Figure S14). Interestingly, we identified RDH10 as a new substrate of linear Ub in HEK293T cells treated with TNFα. RDH10 showed both intensive K48-polyUb signals and linear Ub signals in the presence of LUBAC (see Supplementary Figure S14). While co-expression of OTUB1 (a deubiquitinase specific for K48-linked polyUb) disrupted the K48-polyUb signals of RDH10, the linear Ub signals of RDH10 were also significantly decreased (Supplementary Figure S15). This observation indicated that RDH10 probably harbors a K48-/M1-hybrid polyUb chain. The biological functions of this novel substrate RDH10 and its hybrid K48-/M1-polyUb modification are worth further investigation. We are proposing to use adeno-associated virus (AAV) for the delivery of PylRS/$tRNA_{CUA}$ cassettes and unnatural amino acid-engineered Ub. This may extend the application of our approach to *in vivo* settings.

DATA AVAILABILITY

The mass spectrometry proteomics data have been deposited in the ProteomeXchange Consortium (http://proteomecentral.proteomexchange.org) via the iProX partner repository with the dataset identifier PXD031600.

SUPPLEMENTARY DATA

Supplementary Data are available at NAR Online.

ACKNOWLEDGEMENTS

We thank Professor Demin Zhou (Peking University) for providing the 7SK-tRNA-PylRS vector and MbPylRS-tRNA system, and Professor Jeremy N. Rich (University of California San Diego) for providing glioblastoma cell lines. We also thank Professor Hu Zhou (Shanghai Institute of Materia Medica, CAS) and Dr Fang Liu (State Key Laboratory of Proteomics, Beijing) for mass spectrometry analysis.

Author contributions: X.D., B.W., T.Z., A-L.L., J.-H.M. and H.-Y.L. supervised the project. X.D. and B.W. designed the study. X.-L.D., J.P., M.W., Y.C., Z.-C.W., N.W., T.-Q.L. and T.S. performed biochemistry and biological experiments. X.D. and X.-L.D. performed mass spectrometry analysis. J.N.F. performed computational simulation and structural analysis. X.D., B.W., J.P., B.G. and X.-L.D. analyzed the data. X.D., B.W. and X.-L.D. wrote the manuscript.

FUNDING

This work was supported by National Science and Technology Major Projects for New Drugs Innovation and Development [2019ZX09J19105] and the National Natural Science Foundation of China [81302739].

Conflict of interest statement. None declared.

REFERENCES

1. Kirisako,T., Kamei,K., Murata,S., Kato,M., Fukumoto,H., Kanie,M., Sano,S., Tokunaga,F., Tanaka,K. and Iwai,K. (2006) A ubiquitin ligase complex assembles linear polyubiquitin chains. *EMBO J.*, **25**, 4877–4887.
2. Tokunaga,F., Sakata,S., Saeki,Y., Satomi,Y., Kirisako,T., Kamei,K., Nakagawa,T., Kato,M., Murata,S., Yamaoka,S. *et al.* (2009) Involvement of linear polyubiquitylation of NEMO in NF-kappaB activation. *Nat. Cell Biol.*, **11**, 123–132.
3. Ikeda,F., Deribe,Y.L., Skånland,S.S., Stieglitz,B., Grabbe,C., Franz-Wachtel,M., van Wijk,S.J., Goswami,P., Nagy,V., Terzic,J. *et al.* (2011) SHARPIN forms a linear ubiquitin ligase complex regulating NF-κB activity and apoptosis. *Nature*, **471**, 637–641.
4. Gerlach,B., Cordier,S.M., Schmukle,A.C., Emmerich,C.H., Rieser,E., Haas,T.L., Webb,A.I., Rickard,J.A., Anderton,H., Wong,W.W. *et al.* (2011) Linear ubiquitination prevents inflammation and regulates immune signalling. *Nature*, **471**, 591–596.
5. Keusekotten,K., Elliott,P.R., Glockner,L., Fiil,B.K., Damgaard,R.B., Kulathu,Y., Wauer,T., Hospenthal,M.K., Gyrd-Hansen,M., Krappmann,D. *et al.* (2013) OTULIN antagonizes LUBAC signaling by specifically hydrolyzing Met1-linked polyubiquitin. *Cell*, **153**, 1312–1326.
6. Rivkin,E., Almeida,S.M., Ceccarelli,D.F., Juang,Y.C., MacLean,T.A., Srikumar,T., Huang,H., Dunham,W.H., Fukumura,R., Xie,G. *et al.* (2013) The linear ubiquitin-specific deubiquitinase gumby regulates angiogenesis. *Nature*, **498**, 318–324.

7. Fiil,B.K., Damgaard,R.B., Wagner,S.A., Keusekotten,K., Fritsch,M., Bekker-Jensen,S., Mailand,N., Choudhary,C., Komander,D. and Gyrd-Hansen,M. (2013) OTULIN restricts Met1-linked ubiquitination to control innate immune signaling. *Mol. Cell*, **50**, 818–830.
8. Hrdinka,M. and Gyrd-Hansen,M. (2017) The Met1-linked ubiquitin machinery: emerging themes of (De)regulation. *Mol. Cell*, **68**, 265–280.
9. Rahighi,S., Ikeda,F., Kawasaki,M., Akutsu,M., Suzuki,N., Kato,R., Kensche,T., Uejima,T., Bloor,S., Komander,D. *et al.* (2009) Specific recognition of linear ubiquitin chains by NEMO is important for NF-kappaB activation. *Cell*, **136**, 1098–1109.
10. Rodgers,M.A., Bowman,J.W., Fujita,H., Orazio,N., Shi,M., Liang,Q., Amatya,R., Kelly,T.J., Iwai,K., Ting,J. *et al.* (2014) The linear ubiquitin assembly complex (LUBAC) is essential for NLRP3 inflammasome activation. *J. Exp. Med.*, **211**, 1333–1347.
11. Wei,R., Xu,L.W., Liu,J., Li,Y., Zhang,P., Shan,B., Lu,X., Qian,L., Wu,Z., Dong,K. *et al.* (2017) SPATA2 regulates the activation of RIPK1 by modulating linear ubiquitination. *Genes Dev.*, **31**, 1162–1176.
12. Zuo,Y., Feng,Q., Jin,L., Huang,F., Miao,Y., Liu,J., Xu,Y., Chen,X., Zhang,H., Guo,T. *et al.* (2020) Regulation of the linear ubiquitination of STAT1 controls antiviral interferon signaling. *Nat. Commun.*, **11**, 1146.
13. Wu,M., Chang,Y., Hu,H., Mu,R., Zhang,Y., Qin,X., Duan,X., Li,W., Tu,H., Zhang,W. *et al.* (2019) LUBAC controls chromosome alignment by targeting CENP-E to attached kinetochores. *Nat. Commun.*, **10**, 273.
14. Matsumoto,M.L., Dong,K.C., Yu,C., Phu,L., Gao,X., Hannoush,R.N., Hymowitz,S.G., Kirkpatrick,D.S., Dixit,V.M. and Kelley,R.F. (2012) Engineering and structural characterization of a linear polyubiquitin-specific antibody. *J. Mol. Biol.*, **418**, 134–144.
15. Sasaki,Y., Sano,S., Nakahara,M., Murata,S., Kometani,K., Aiba,Y., Sakamoto,S., Watanabe,Y., Tanaka,K., Kurosaki,T. *et al.* (2013) Defective immune responses in mice lacking LUBAC-mediated linear ubiquitination in B cells. *EMBO J.*, **32**, 2463–2476.
16. Kliza,K., Taumer,C., Pinzuti,I., Franz-Wachtel,M., Kunzelmann,S., Stieglitz,B., Macek,B. and Husnjak,K. (2017) Internally tagged ubiquitin: a tool to identify linear polyubiquitin-modified proteins by mass spectrometry. *Nat. Methods*, **14**, 504–512.
17. Man,J., Yu,X., Huang,H., Zhou,W., Xiang,C., Huang,H., Miele,L., Liu,Z., Bebek,G., Bao,S. *et al.* (2018) Hypoxic induction of vasorin regulates Notch1 turnover to maintain glioma stem-like cells. *Cell Stem Cell*, **22**, 104–118.
18. Zhan,X., Guo,S., Li,Y., Ran,H., Huang,H., Mi,L., Wu,J., Wang,X., Xiao,D., Chen,L. *et al.* (2020) Glioma stem-like cells evade interferon suppression through MBD3/NuRD complex-mediated STAT1 downregulation. *J. Exp. Med.*, **217**, e20191340.
19. Si,L., Xu,H., Zhou,X., Zhang,Z., Tian,Z., Wang,Y., Wu,Y., Zhang,B., Niu,Z., Zhang,C. *et al.* (2016) Generation of influenza A viruses as live but replication-incompetent virus vaccines. *Science*, **354**, 1171.
20. Yan,F., Huang,C., Wang,X., Tan,J., Cheng,S., Wan,M., Wang,Z., Wang,S., Luo,S., Li,A. *et al.* (2020) Threonine ADP-ribosylation of ubiquitin by a bacterial effector family blocks host ubiquitination. *Mol. Cell*, **78**, 641–652.
21. Guryanova,O.A., Wu,Q., Cheng,L., Lathia,J.D., Huang,Z., Yang,J., MacSwords,J., Eyler,C.E., McLendon,R.E., Heddleston,J.M. *et al.* (2011) Nonreceptor tyrosine kinase BMX maintains self-renewal and tumorigenic potential of glioblastoma stem cells by activating STAT3. *Cancer Cell*, **19**, 498–511.
22. Tyanova,S., Temu,T. and Cox,J. (2016) The MaxQuant computational platform for mass spectrometry-based shotgun proteomics. *Nat. Protoc.*, **11**, 2301–2319.
23. Smit,J.J., Monteferrario,D., Noordermeer,S.M., van Dijk,W.J., van der Reijden,B.A. and Sixma,T.K. (2012) The E3 ligase HOIP specifies linear ubiquitin chain assembly through its RING-IBR-RING domain and the unique LDD extension. *EMBO J.*, **31**, 3833–3844.
24. Chin,J.W., Cropp,T.A., Anderson,J.C., Mukherji,M., Zhang,Z. and Schultz,P.G. (2003) An expanded eukaryotic genetic code. *Science*, **301**, 964–967.
25. Hong,S., Hwang,D.Y., Yoon,S., Isacson,O., Ramezani,A., Hawley,R.G. and Kim,K.S. (2007) Functional analysis of various promoters in lentiviral vectors at different stages of in vitro differentiation of mouse embryonic stem cells. *Mol. Ther.*, **15**, 1630–1639.
26. Shen,B., Xiang,Z., Miller,B., Louie,G., Wang,W., Noel,J.P., Gage,F.H. and Wang,L. (2011) Genetically encoding unnatural amino acids in neural stem cells and optically reporting voltage-sensitive domain changes in differentiated neurons. *Stem Cells*, **29**, 1231–1240.
27. Mbua,N.E., Guo,J., Wolfert,M.A., Steet,R. and Boons,G.J. (2011) Strain-promoted alkyne–azide cycloadditions (SPAAC) reveal new features of glycoconjugate biosynthesis. *Chembiochem*, **12**, 1912–1921.
28. Tokunaga,F., Sakata,S.-i., Saeki,Y., Satomi,Y., Kirisako,T., Kamei,K., Nakagawa,T., Kato,M., Murata,S., Yamaoka,S. *et al.* (2009) Involvement of linear polyubiquitylation of NEMO in NF-κB activation. *Nat. Cell Biol.*, **11**, 123–132.
29. Heger,K., Wickliffe,K.E., Ndoja,A., Zhang,J., Murthy,A., Dugger,D.L., Maltzman,A., Melo,F.d.S., Hung,J., Zeng,Y. *et al.* (2018) OTULIN limits cell death and inflammation by deubiquitinating LUBAC. *Nature*, **559**, 120–124.
30. Inn,K.S., Gack,M.U., Tokunaga,F., Shi,M., Wong,L.Y., Iwai,K. and Jung,J.U. (2011) Linear ubiquitin assembly complex negatively regulates RIG-I- and TRIM25-mediated type I interferon induction. *Mol. Cell*, **41**, 354–365.
31. Goto,E. and Tokunaga,F. (2017) Decreased linear ubiquitination of NEMO and FADD on apoptosis with caspase-mediated cleavage of HOIP. *Biochem. Biophys. Res. Commun.*, **485**, 152–159.
32. Zhang,H., Zhao,X., Guo,Y., Chen,R., He,J., Li,L., Qiang,Z., Yang,Q., Liu,X., Huang,C. *et al.* (2021) Hypoxia regulates overall mRNA homeostasis by inducing Met(1)-linked linear ubiquitination of AGO2 in cancer cells. *Nat. Commun.*, **12**, 5416.
33. Noad,J., von der Malsburg,A., Pathe,C., Michel,M.A., Komander,D. and Randow,F. (2017) LUBAC-synthesized linear ubiquitin chains restrict cytosol-invading bacteria by activating autophagy and NF-κB. *Nat. Microbiol.*, **2**, 17063.
34. van Wijk,S.J.L., Fricke,F., Herhaus,L., Gupta,J., Hötte,K., Pampaloni,F., Grumati,P., Kaulich,M., Sou,Y.S., Komatsu,M. *et al.* (2017) Linear ubiquitination of cytosolic *Salmonella typhimurium* activates NF-κB and restricts bacterial proliferation. *Nat. Microbiol.*, **2**, 17066.
35. Brazee,P.L., Morales-Nebreda,L., Magnani,N.D., Garcia,J.G., Misharin,A.V., Ridge,K.M., Budinger,G.R.S., Iwai,K., Dada,L.A. and Sznajder,J.I. (2020) Linear ubiquitin assembly complex regulates lung epithelial-driven responses during influenza infection. *J. Clin. Invest.*, **130**, 1301–1314.
36. Wertz,I.E., Newton,K., Seshasayee,D., Kusam,S., Lam,C., Zhang,J., Popovych,N., Helgason,E., Schoeffler,A., Jeet,S. *et al.* (2015) Phosphorylation and linear ubiquitin direct A20 inhibition of inflammation. *Nature*, **528**, 370–375.
37. Tao,P., Wang,S., Ozen,S., Lee,P.Y., Zhang,J., Wang,J., Han,H., Yang,Z., Fang,R., Tsai,W.L. *et al.* (2021) Deubiquitination of proteasome subunits by OTULIN regulates type I IFN production. *Sci. Adv.*, **7**, eabi6794.
38. van Well,E.M., Bader,V., Patra,M., Sánchez-Vicente,A., Meschede,J., Furthmann,N., Schnack,C., Blusch,A., Longworth,J., Petrasch-Parwez,E. *et al.* (2019) A protein quality control pathway regulated by linear ubiquitination. *EMBO J.*, **38**, e100730.
39. Garner,J.M., Fan,M., Yang,C.H., Du,Z., Sims,M., Davidoff,A.M. and Pfeffer,L.M. (2013) Constitutive activation of signal transducer and activator of transcription 3 (STAT3) and nuclear factor κb signaling in glioblastoma cancer stem cells regulates the Notch pathway. *J. Biol. Chem.*, **288**, 26167–26176.
40. Yamamoto,T., Sekine,Y., Kashima,K., Kubota,A., Sato,N., Aoki,N. and Matsuda,T. (2002) The nuclear isoform of protein-tyrosine phosphatase TC-PTP regulates interleukin-6-mediated signaling pathway through STAT3 dephosphorylation. *Biochem. Biophys. Res. Commun.*, **297**, 811–817.
41. Wang,Y., Ning,H., Ren,F., Zhang,Y., Rong,Y., Wang,Y., Su,F., Cai,C., Jin,Z., Li,Z. *et al.* (2014) GdX/UBL4A specifically stabilizes the TC45/STAT3 association and promotes dephosphorylation of STAT3 to repress tumorigenesis. *Mol. Cell*, **53**, 752–765.
42. Sang,Y., Li,Y., Song,L., Alvarez,A.A., Zhang,W., Lv,D., Tang,J., Liu,F., Chang,Z., Hatakeyama,S. *et al.* (2018) TRIM59 promotes gliomagenesis by inhibiting TC45 dephosphorylation of STAT3. *Cancer Res.*, **78**, 1792–1804.

43. Yu,H., Pardoll,D. and Jove,R. (2009) STATs in cancer inflammation and immunity: a leading role for STAT3. *Nat. Rev. Cancer*, **9**, 798–809.
44. Zhong,Z., Wen,Z. and Darnell,J.E. Jr. (1994) Stat3: a STAT family member activated by tyrosine phosphorylation in response to epidermal growth factor and interleukin-6. *Science*, **264**, 95–98.
45. Kim,E., Kim,M., Woo,D.H., Shin,Y., Shin,J., Chang,N., Oh,Y.T., Kim,H., Rheey,J., Nakano,I. *et al.* (2013) Phosphorylation of EZH2 activates STAT3 signaling via STAT3 methylation and promotes tumorigenicity of glioblastoma stem-like cells. *Cancer Cell*, **23**, 839–852.
46. Zhang,M., Zhou,L., Xu,Y., Yang,M., Xu,Y., Komaniecki,G.P., Kosciuk,T., Chen,X., Lu,X., Zou,X. *et al.* (2020) A STAT3 palmitoylation cycle promotes T(H)17 differentiation and colitis. *Nature*, **586**, 434–439.
47. Hospenthal,M.K., Mevissen,T.E.T. and Komander,D. (2015) Deubiquitinase-based analysis of ubiquitin chain architecture using Ubiquitin Chain Restriction (UbiCRest). *Nat. Protoc.*, **10**, 349–361.